Supplementary Information: Strain Engineering of Nonlinear Nanoresonators from Hardening to Softening

Zichao Li*[1], Minxing Xu[1,2], Richard A. Norte[1,2], Alejandro M. Aragón[1], Peter G. Steeneken[1,2], and Farbod Alijani*[1]

[1]Department of Precision and Microsystems Engineering, Delft University of Technology, Mekelweg 2, 2628 CD Delft, The Netherlands

[2]Kavli Institute of Nanoscience, Delft University of Technology, Lorentzweg 1, 2628 CJ Delft, The Netherlands

September 11, 2023

S1. Fitting the backbone of multiple frequency response curves

Here we discuss our fitting strategy to find the Duffing constant k_3 of the string resonators from frequency sweeps at different drive levels. We note that the resonance frequencies of nanomechanical resonators with high stress are sensitive to temperature variations. Both the measurement laser and the environment can induce thermal variations which may cause the resonance frequency of our resonators to drift few tens of hertz during consecutive frequency sweep measurements under different drive levels. This in turn can make the estimation of the Duffing constant very difficult. In order to correct for this, we first fit the off-resonance response of multiple frequency response curves at different drive levels to estimate the resonance frequency f_0 using the damped harmonic oscillator model:

$$A_{\mathrm{meas}} = \frac{\dfrac{A_{\max}}{Q}}{\sqrt{\left[1-\left(\dfrac{f}{f_0}\right)^2\right]^2+\left(\dfrac{1}{Q}\dfrac{f}{f_0}\right)^2}}, \tag{S1}$$

where A_{meas} is the measured amplitude of the string at its center, $A_{\max}$ is the maximum A_{meas} of each frequency sweep, and f is the drive frequency, as shown in Fig. S1a. To be able to estimate k_3 from the backbone, we then fix the response curve of the lowest drive level and horizontally adjust all the other curves at higher drive levels, according to the differences between their linearly fitted f_0 and the one of the lowest drive level (see blue arrows in Fig. S1a). This would allow us to extract the Duffing constant with good accuracy from multiple frequency response curves at difference drive levels, as shown in Fig. S1b.

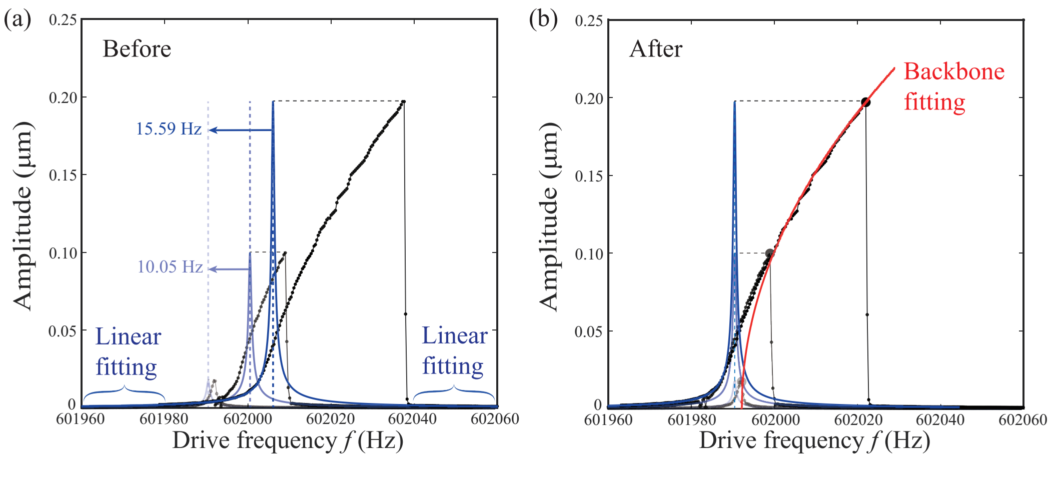

Figure S1: **Fitting the backbone of multiple frequency response curves.** We choose three frequency sweeps (black lines with dots) from the string resonator with $w_s = 1\,\mu\mathrm{m}$, $L_s = 150\,\mu\mathrm{m}$ and $\theta = 0.3\,\mathrm{rad}$ to demonstrate the methodology. The red curve shows the backbone fitted by multiple frequency sweeps after adjusting the resonance frequency. The blue curves show the linear fits using the off-resonance response of the nonlinear resonance curves at different drive levels.

S2. Nonlinear dynamics of a string with compliant supports

Here we obtain the equations of motion of a string resonator with complaint support and finite in-plane stiffness k_i at its two ends.

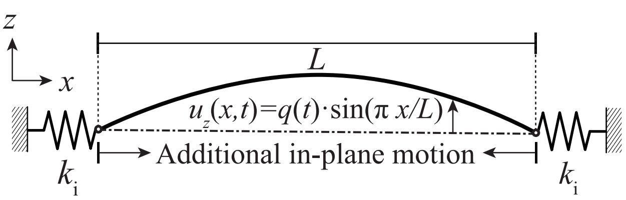

Figure S2: **Simplified model for a string resonator with compliant supports.** The influence from supports on the geometric nonlinearity is equivalent to a pair of in-plane translational springs, which relaxes the in-plane stiffening when the string vibrates at large amplitudes.

Assuming the string vibrates in its out-of-plane fundamental mode, we assume the motion to be of the form:

$$\begin{aligned} u_z(x,t) &= q(t)\sin\left(\frac{\pi}{L}x\right), \\ u_x(x,t) &= u_{x,0}(x,t) + q_\mathrm{a}(t)\left(1-\frac{2x}{L}\right) \\ &= q_0\left(\frac{2x}{L}-1\right) + \sum_{i=1}^{N} q_i(t)\sin\left(\frac{2i\pi x}{L}\right) + q_\mathrm{a}(t)\left(1-\frac{2x}{L}\right), \end{aligned} \tag{S2}$$

where u_x and u_z are the displacements of the string in x (in-plane) and z (out-of-plane) directions, respectively. $u_{x,0}(x,t)$ represents the in-plane counterpart of a stressed doubly clamped string under the out-of-plane motion $u_z(x,t)$. $q_\mathrm{a}(t)$ is the additional in-plane motion caused by the finite k_i. q_0 is a constant to represent the initial stress in x direction of the string:

$$q_0 = \frac{(1-\nu)\sigma_0 L}{2E}, \tag{S3}$$

$q_\mathrm{a}(t)$ in Eq. (S2) is the additional in-plane degrees-of-freedom that is considered to ensure satisfaction of the boundary conditions and can be obtained as:

$$\begin{aligned} k_\mathrm{i} q_\mathrm{a}(t) &= \frac{EA}{L}\int_0^{\frac{L}{2}} \varepsilon \mathrm{d}x \\ &= \frac{EA}{L}\int_0^{\frac{L}{2}} \left[\frac{\partial u_x}{\partial x} + \frac{1}{2}\left(\frac{\partial u_z}{\partial x}\right)^2\right]\mathrm{d}x, \end{aligned} \tag{S4}$$

where $A = hw$ is the area of the string's cross section and ε is the strain along the x direction. Then by substituting Eq. (S2) in Eq. (S4) we have:

$$q_\mathrm{a}(t) = \frac{\pi^2 q^2(t)}{8L}\left(1+\frac{k_\mathrm{i}L}{2EA}\right)^{-1}. \tag{S5}$$

The strain energy of a string can be written as:

$$U_\mathrm{s} = \frac{1}{2}\int_0^L EA\varepsilon^2 \mathrm{d}x. \tag{S6}$$

The energy stored in the two in-plane springs k_i is:

$$U_\mathrm{k} = 2\times\frac{1}{2}k_\mathrm{i}q_\mathrm{a}^2(t). \tag{S7}$$

Furthermore, the kinetic energy of the string neglecting the in-plane inertia is given by:

$$T = \frac{1}{2}\rho A\int_0^L \left(\frac{\partial u_z}{\partial t}\right)^2 \mathrm{d}x. \tag{S8}$$

Using Eq. (S6 - S8), the Lagrange equations can be constructed as:

$$\frac{\mathrm{d}}{\mathrm{d}t}\left(\frac{\partial T}{\partial \dot{\boldsymbol{q}}}\right) - \frac{\partial T}{\partial \boldsymbol{q}} + \frac{\partial U}{\partial \boldsymbol{q}} = \frac{\partial W}{\partial \boldsymbol{q}}, \tag{S9}$$

where $\boldsymbol{q} = [q(t), q_i(t)], i = 1, 2, ..., N$, is the vector that includes all the generalized coordinates. Since the in-plane inertia has been neglected, after substituting the potential energy $U = U_\mathrm{s} + U_\mathrm{k}$ and the kinetic energy T in Eq. S10, we have a system of nonlinear equations consisting of a single differential equation associated with the generalized coordinate $q(t)$ and N algebraic equations in terms of $q_i(t)$. By solving the N algebraic equations we can determine $q_i(t)$ in terms of $q(t)$:

$$\begin{aligned} q_1(t) &= -\frac{\pi q^2(t)}{8L} \\ q_2(t) &= q_3(t) = ... = q_N(t) = 0, \end{aligned} \tag{S10}$$

which will reduce the $N+1$ nonlinear equations to a single Duffing equation:

$$\ddot{q} + c\dot{q} + k_1 q + k_3 q^3 = F_\mathrm{exc}\sin(2\pi f t). \tag{S11}$$

The mass-normalized linear stiffness k_1 and the Duffing constant k_3 are:

$$k_1 = \frac{\pi^2(1-\nu)\sigma_0}{\rho L^4}\left(1 + \frac{2EA}{k_\mathrm{i}L}\right)^{-1}, \tag{S12}$$

$$k_3 = \frac{\pi^4 E}{4\rho L^4}\left(1 + \frac{2EA}{k_\mathrm{i}L}\right)^{-1}, \tag{S13}$$

from which we can conclude that k_1 and k_3 increase with the increasing k_i. According to the expression of k_1, we can obtain the resonance frequency of the assumed mode shape as:

$$f_0 = \frac{1}{2L}\sqrt{\frac{1}{\rho}\frac{(1-\nu)\sigma_0}{1+\frac{2EA}{k_\mathrm{i}L}}} = \frac{1}{2L}\sqrt{\frac{\sigma_\mathrm{b}}{\rho}}, \tag{S14}$$

where σ_b is the stress of the string in x direction after the release etch [2]:

$$\sigma_\mathrm{b} = (1-\nu)\sigma_0\left(1 + \frac{2EA}{k_\mathrm{i}L}\right)^{-1}. \tag{S15}$$

It is worth noting that $(1 + 2EA/k_\mathrm{i}L)^{-1}$ serves as a tuning factor introduced by the finite in-plane stiffness k_i, which rescales σ_b, k_1 and k_3 of a doubly clamped string with pre-tension $(1-\nu)\sigma_0$ in the same rate. The additional infinite k_i will relax the pre-tention as shown in Eq. (S15). Consequently, the linear stiffness $k_1 = (2\pi f_0)^2$ which is proportional to the tension, is scaled down for $(1 + 2EA/k_\mathrm{i}L)^{-1}$. In contrast, the finite in-plane springs k_i rescale the Duffing constant k_3 in a different way that they bring an additional in-plane motion $q_\mathrm{a}(t)\,(1 - 2x/L)$ along with $u_{x,0}(x,t)$ as shown in Eq. (S2), to neutralize the elongation of the central string under large-amplitude vibrations. Surprisingly, k_3 is scaled down at the same rate, i.e. the tuning factor $(1 + 2EA/k_\mathrm{i}L)^{-1}$ of σ_b and k_1, which is demonstrated by the solid line in Fig. S3a and Fig. S3b. The dotted lines in Fig. S3 show the analytical results of a doubly fixed string under different σ_b, which show an opposite trend against σ_b compared to the ones with soft-clamping. The measurement results of softly clamped strings (diamonds) with different σ_b (by varying w_s and L_s, same devices in Fig. 2), as well as the doubly clamped string (star) are also demonstrated in Fig. S3, which further validate our simplified model.

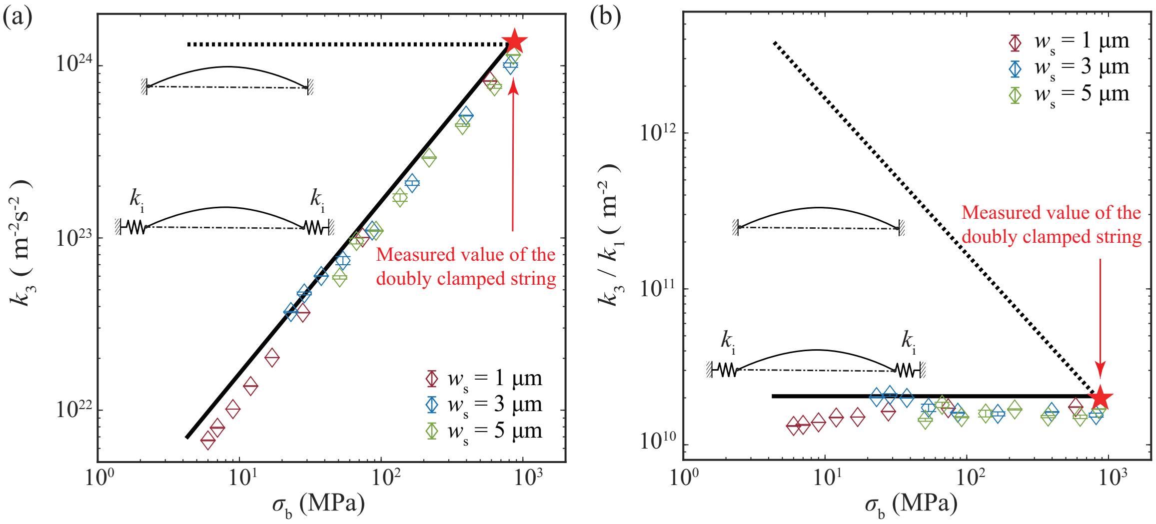

Figure S3: **Dependence of linear and nonlinear stiffness on stress σ_b tuned by supports' in-plane stiffness k_i.** The solid lines represent the strings with finite stiffness k_i and the dotted lines are results of doubly clamped strings.

S3. Reduced-order modeling of finite element simulation

We perform our finite element (FE) simulations with commerical FE software COMSOL. We first perform static analysis of the strained structures to calculate the stress redistribution and the static deformation. For devices with negative support angles θ, we perform an additional buckling analysis to obtain the buckled state. This procedure mimics the etching process that the high-stress Si_3N_4 layer releases from the silicon substrate. It is worth noting that the high initial stress of the structure will lead to deformation of the device compared to its unreleased state. In order to calculate nonlinear forces with good accuracy, we thus first calculate this initial deformed state and only afterwards perform eigenfrequency analysis. The full FE model for the deformed configuration is then written as:

$$\boldsymbol{M}\ddot{\boldsymbol{X}}(t) + \boldsymbol{C}\dot{\boldsymbol{X}}(t) + \boldsymbol{K}\boldsymbol{X}(t) + \boldsymbol{\Gamma}(\boldsymbol{X}(t)) = \boldsymbol{F}(t), \tag{S16}$$

where $\boldsymbol{M}$, $\boldsymbol{C}$, $\boldsymbol{K}$ are the mass, damping, and linear stiffness (considering the additional stiffness from the redistributed stress field as well) matrices, respectively, and $\boldsymbol{X}(t)$ is the displacement vector and $\boldsymbol{F}(t)$ is the vector of drive force in physical coordinates. $\boldsymbol{\Gamma}(\boldsymbol{X}(t))$ represents the nonlinear force vector due to geometric nonlinearity which is in this work composed of the quadratic and cubic terms of $\boldsymbol{X}(t)$. We use the eigenvectors' of Eq. (S16) to obtain a set of N symmetric out-of-plane modes $\boldsymbol{\Phi}$ as the assumption of displacement fields for the STiffness Evaluation Procedure (STEP) [1], which is the reduced-order model (ROM) technique we use to capture the geometric nonlinearity. A set of coupled modal equations with reduced degrees-of-freedom are then obtained by applying the modal coordinate transformation $\boldsymbol{X}(t) = \boldsymbol{\Phi}\boldsymbol{q}(t)$:

$$\widetilde{\boldsymbol{M}}\ddot{\boldsymbol{q}}(t) + \widetilde{\boldsymbol{C}}\dot{\boldsymbol{q}}(t) + \widetilde{\boldsymbol{K}}\boldsymbol{q}(t) + \boldsymbol{\gamma}(\boldsymbol{q}(t)) = \widetilde{\boldsymbol{F}}(t), \tag{S17}$$

where $\widetilde{\boldsymbol{M}} = \boldsymbol{\Phi}^{\mathrm{T}}\boldsymbol{M}\boldsymbol{\Phi}$, $\widetilde{\boldsymbol{C}} = \boldsymbol{\Phi}^{\mathrm{T}}\boldsymbol{C}\boldsymbol{\Phi}$, $\widetilde{\boldsymbol{K}} = \boldsymbol{\Phi}^{\mathrm{T}}\boldsymbol{K}\boldsymbol{\Phi}$, $\boldsymbol{\gamma}(\boldsymbol{q}(t)) = \boldsymbol{\Phi}^{\mathrm{T}}\boldsymbol{\Gamma}(\boldsymbol{X}(t))$, $\widetilde{\boldsymbol{F}} = \boldsymbol{\Phi}^{\mathrm{T}}\boldsymbol{F}$. $\boldsymbol{q}(t)$ is the set of N modal coordinates which contains $q_1(t), q_2(t), ..., q_{\mathrm{N}}(t)$. The nonlinear term $\boldsymbol{\gamma}(\boldsymbol{q}(t))$ can be detailed as:

$$\gamma^{(i)} = \sum_{j=1}^{N}\sum_{k=j}^{N}\alpha_{jk}^{(i)} q_j q_k + \sum_{j=1}^{N}\sum_{k=j}^{N}\sum_{l=k}^{N}\beta_{jkl}^{(i)} q_j q_k q_l, \tag{S18}$$

where i represents the ith modal coordinate and j, k, l are mode numbers. Based on the prescribed displacement fields, we solve for the reaction forces on all elements with and without considering the geometric nonlinearity in the full FE model, i.e. $\boldsymbol{F}_{\mathrm{total}}(= \boldsymbol{F}_{\mathrm{linear}} + \boldsymbol{F}_{\mathrm{nonlinear}})$ and $\boldsymbol{F}_{\mathrm{linear}}$, respectively. Then we can project the obtained reaction force vectors in physical coordinates to the ith modal coordinate, and calculate the nonlinear reaction force $\gamma^{(i)} = F_{\mathrm{nonlinear}}^{(i)} = F_{\mathrm{total}}^{(i)} - F_{\mathrm{linear}}^{(i)}$. Consequently, by applying different combinations of modal coordinates $q_1(t), q_2(t), ..., q_{\mathrm{N}}(t)$ as the displacement field, we extract the corresponding modal nonlinear reaction forces. With a set of algebraic equations in the form of Eq. (S18), we solve for the quadratic coefficient α and the cubic coefficient β for all modal coordinates. Meanwhile, according to the static stress field and the eigenvectors $\boldsymbol{\Phi}$ (mode shapes), Q-factors of all modal coordinates can be calculated [2]. Finally, we assemble Eq. (S17) and calculate the response of the ROM under different drives by numerical continuation (Matcont [3]).

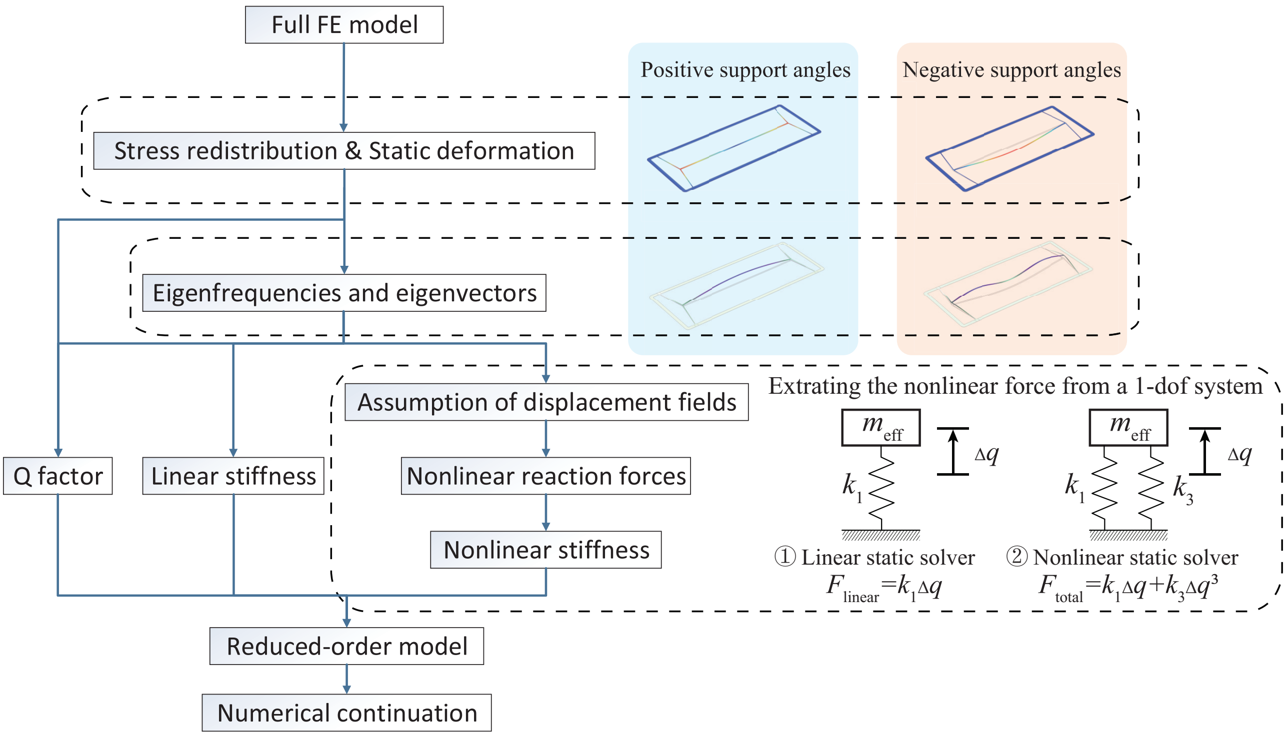

Figure S4: **The flowchart of the reduced-order modeling procedure.** The static analysis and eigenfrequency analysis of both flat and buckled devices are shown respectively in blue and orange. An example for a one degree-of-freedom (1-dof) system is shown to demonstate the calculation procedure of the nonlinear reaction force.

For devices dominated by tensile stress, the single-mode ROM works very well as shown in Fig. 4(c) of the main text. For buckled devices which have out-of-plane curvatures and more complex stress field, as shown in Fig. S5b, we use multi-mode ROM to capture the softening nonlinear behavior at large amplitudes. In Fig. S5a, we show the convergence analysis performed to capture the softening behavior. This procedure involves the inclusion of higher modes of vibration in the reduced-order model (Eq. (S17)) until the solution is converged. We note that in-plane modes and asymmetric out-of-plane modes do not have an influential role on the convergence of the obtained nonlinear dynamic responses. We found that building a ROM with only the first mode for the flat ($\theta > 0$) and with the first 6 symmetric eigenmodes for the buckled resonators ($\theta < 0$) is enough to find accurate nonlinear frequency response curves. It is also worth mentioning that for θ around -0.1 rad, the ROM faced numerical instability which was due to string being at snap-through condition. To compare the strength of nonlinearity of the simulated curved with those from experiments, we fit the numerical frequency response curves with the Duffing equation to obtain an effective Duffing constant k_3. The values of these effective k_3 are what we have brought in Fig. 4c of the main text.

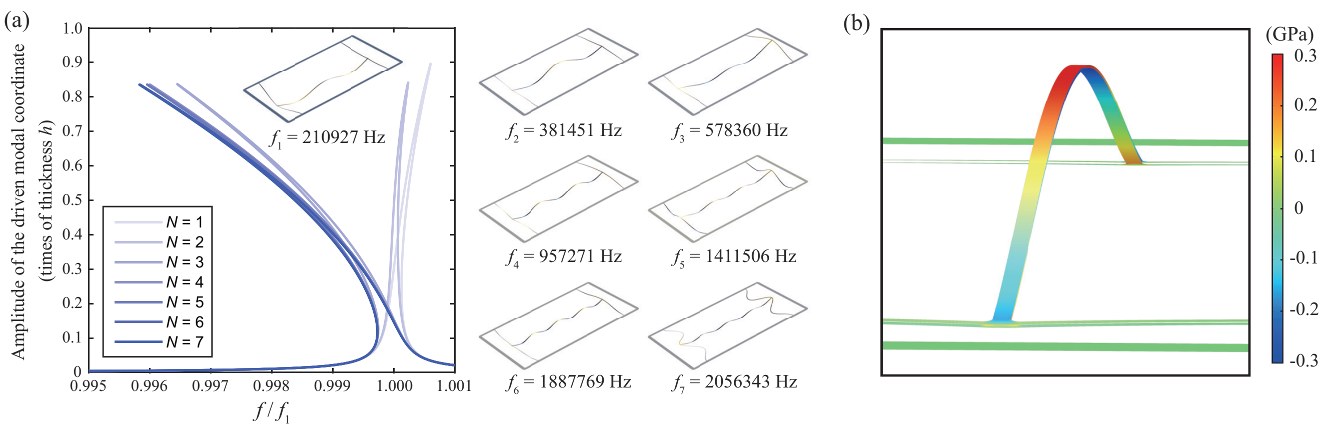

Figure S5: (a) Frequency response of the first symmetric out-of-plane mode (210927Hz) of the device with $L = 200\,\mu\text{m}$, $w = 2\,\mu\text{m}$, $w_s = 1\,\mu\text{m}$, $L_s = 150\,\mu\text{m}$ and $\theta = -0.1\text{rad}$ simulated by Matcont with different numbers of symmetric out-of-plane modes included in the mode set. N refers to the number of modes accounted and modes with lower resonance frequencies are always added with priority. All the modes included in the ROM are listed next to the nonlinear frequency response. (b) The stress field at the top and bottom surface along the length of the string, which is derived after the buckling analysis of the device in (a).

S4. Tunability of $a_{1\mathrm{dB}}$, a_{th} and DR

Using FE simulations and the reduced-order modeling, we perform a parametric study on resonance frequency, Q-factor [2] and the Duffing constant and show the results in Fig. S6a, b and c. It is obvious that all these three parameters could be tuned in a wide range by changing L_{s} and θ of support beams, which work effectively as knobs to tune the dynamics of the resonator with relatively small space occupation and high robustness. Here we only focus on devices with $\theta \geq 0$ because of their high Q-factor and similarity to string resonators.

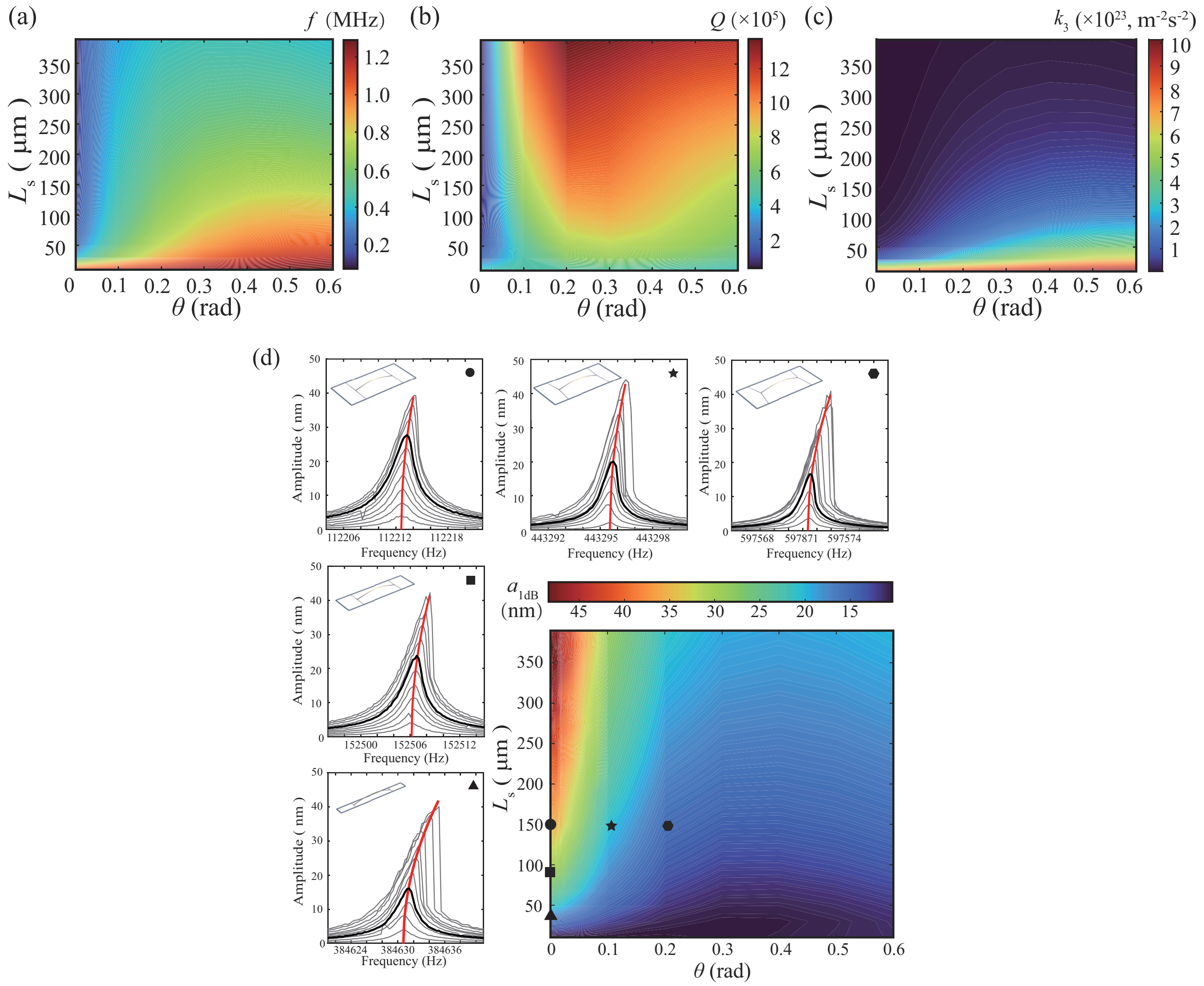

Figure S6: **Tuning dynamical parameters by engineering the supports of string resonators.** FE simulation of (a) fundamental resonance frequency, (b) Q-factor, (c) the Duffing constant k_3 and (d) the onset of nonlinearity $a_{1\mathrm{dB}}$ by varying support design of string resonators with $L = 200\,\mu\mathrm{m}$, $w = 2\,\mu\mathrm{m}$. Five cases are selected to show the measurement of $a_{1\mathrm{dB}}$, where the response curve with closest maximum amplitude compared to $a_{1\mathrm{dB}}$ of each case is bolded.

Based on dynamical parameters shown in Fig. S6a, b and c, we look further into the onset of nonlinearity $a_{1\mathrm{dB}}$ in our resonators, which can be expressed in terms of the Q-factor and the ratio between the linear stiffness k_1 and the Duffing constant (nonlinear stiffness) k_3 [4]:

$$a_{1\mathrm{dB}} = 0.9244\sqrt{\frac{k_1}{Qk_3}}. \tag{S19}$$

We find that support design offers a wide range of tunability along with high fidelity compared to the measurement (see for instance Fig. S6d).

We also investigate the influence of geometric design on the dynamic range DR, which is defined as the ratio between the onset of nonlinearity $a_{1\mathrm{dB}}$ and the thermomechanical noise a_{th} [4]:

$$
\begin{aligned}
\mathrm{DR} &= 20\lg\frac{a_{1\mathrm{dB}}}{a_{\mathrm{th}}} \\
&= 20\lg\frac{0.9244\sqrt{\dfrac{k_1}{Qk_3}}}{\sqrt{\dfrac{4k_{\mathrm{B}}TQ\Delta f}{m_{\mathrm{eff}}k_1^{\frac{3}{2}}}}} \\
&= 20\lg\left[0.4622\left(k_{\mathrm{B}}T\Delta f\right)^{-\frac{1}{2}} m_{\mathrm{eff}}^{-\frac{1}{2}} Q^{-1} k_1^{\frac{5}{4}} k_3^{-\frac{1}{2}}\right],
\end{aligned}
\tag{S20}
$$

where k_{B} is the Boltzmann's constant, T (298K) is the room temperature, Δf (1Hz) is the measurement bandwidth and m_{eff} is the effective mass of the driven mode. In Fig. S7, we demonstrate the FE simulated $a_{1\mathrm{dB}}$, a_{th} and DR of a string resonator with $L = 200\,\mu\mathrm{m}$ and $w = 2\,\mu\mathrm{m}$ against varying support angles θ as well as different support length L_{s} and width w_{s}. The corresponding values of the doubly clamped string without soft-clamping supports are shown as black dotted lines in Fig. S7. In most of the situations, the soft-clamping supports increase the onset of nonlinearity $a_{1\mathrm{dB}}$ and the thermomechanical noise a_{th} at the same time, as a combined result of the increased Q-factor and decreased Duffing constant k_3.

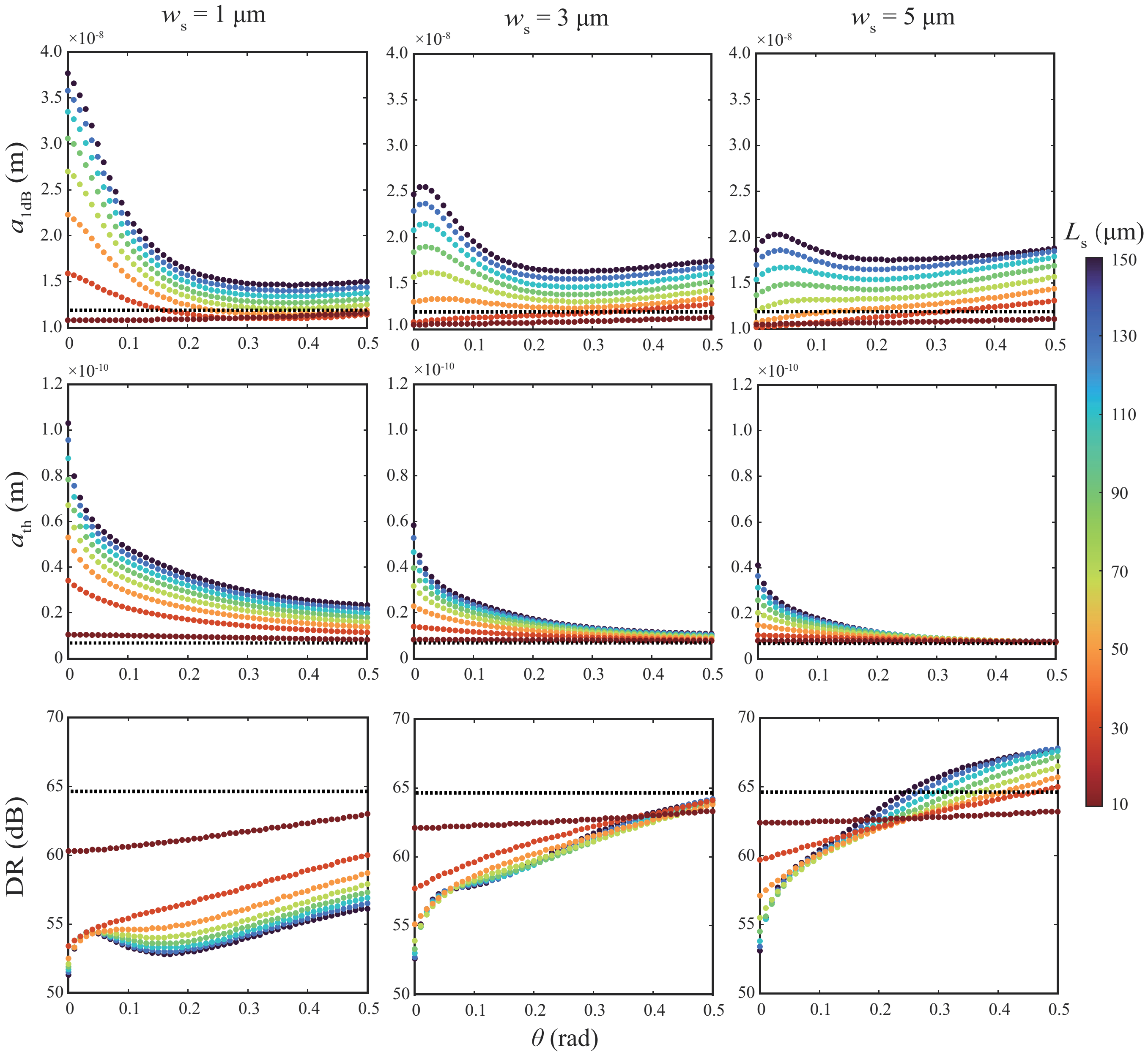

Figure S7: The FE simulated results (colored dots) of the onset of nonlinearity $a_{1\mathrm{dB}}$, thermomechanical noise a_{th} and dynamic range DR of strings with $L = 200\,\mu\mathrm{m}$, $w = 2\,\mu\mathrm{m}$ and three different w_{s} values while varying L_{s} and θ. The corresponding values of a doubly clamped string with $L = 200\,\mu\mathrm{m}$ and $w = 2\,\mu\mathrm{m}$ are plotted as black dotted lines for benchmark, respectively.

As demonstrated by the FE simulations in Fig. S7 and Fig. S8, by reducing the thickness h of our resonators from 340 nm to 20 nm, we can observe a squeezing of DR by 5.5 times, i.e., a reduction of $a_{1\mathrm{dB}}/a_{\mathrm{th}}$ ratio by 450 times. We find an obvious drop in DR of string resonators with supports compared to doubly clamped ones (dotted lines). The squeezing effect for different L_{s} is distinct close to $\theta = 0$ while it saturates as θ and L_{s} become larger. In conclusion, both the small thickness and soft-clamping supports contribute to the realization of thermally driven nonlinear nanomechanical resonators at room temperature.

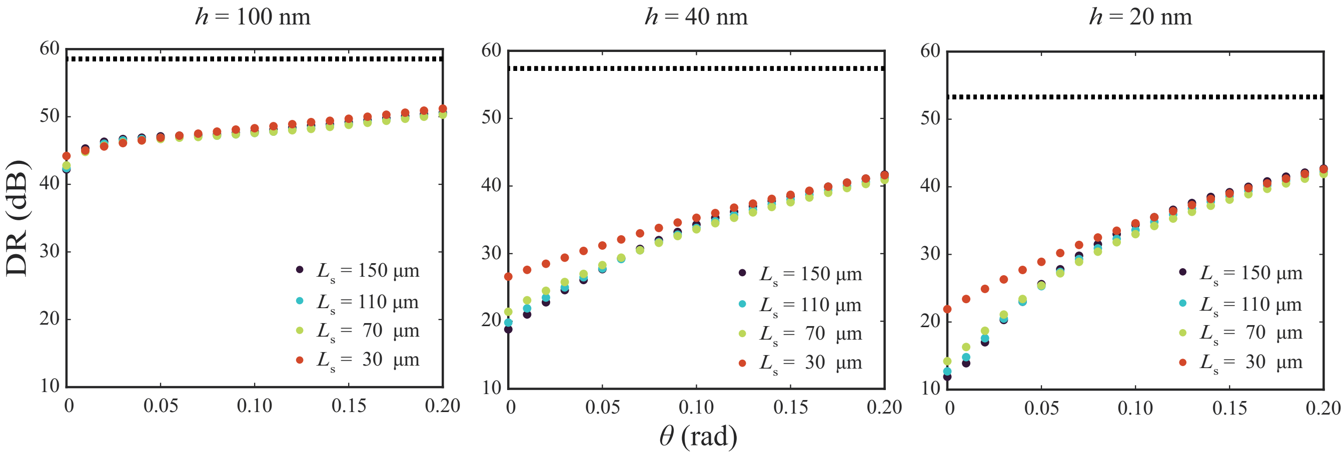

Figure S8: The FE simulated results (colored dots) of the dynamic range DR of strings with $L = 200\,\mu\mathrm{m}$, $w = 2\,\mu\mathrm{m}$, $w_{\mathrm{s}} = 1\,\mu\mathrm{m}$ and three different thickness h values while varying L_{s} and θ. The values of a doubly clamped string with $L = 200\,\mu\mathrm{m}$, $w = 2\,\mu\mathrm{m}$ and corresponding h values are plotted as black dotted lines for benchmark, respectively.

References

[1] A. A. Muravyov and S. A. Rizzi, Determination of nonlinear stiffness with application to random vibration of geometrically nonlinear structures, Computers Structures 81, 1513–1523 (2003).

[2] Z. Li, M. Xu, R. A. Norte, A. M. Aragón, F. van Keulen, F. Alijani, and P. G. Steeneken, Tuning the Q-factor of nanomechanical string resonators by torsion support design, Applied Physics Letters 122, 013501 (2023).

[3] A. Dhooge, W. Govaerts, Y. A. Kuznetsov, H. G. E. Meijer, and B. Sautois, New features of the software matcont for bifurcation analysis of dynamical systems, Mathematical and Computer Modelling of Dynamical Systems 14, 147 (2008).

[4] H. C. Postma, I. Kozinsky, A. Husain, and M. Roukes, Dynamic range of nanotube-and nanowire-based electromechanical systems, Applied Physics Letters 86, 223105 (2005).